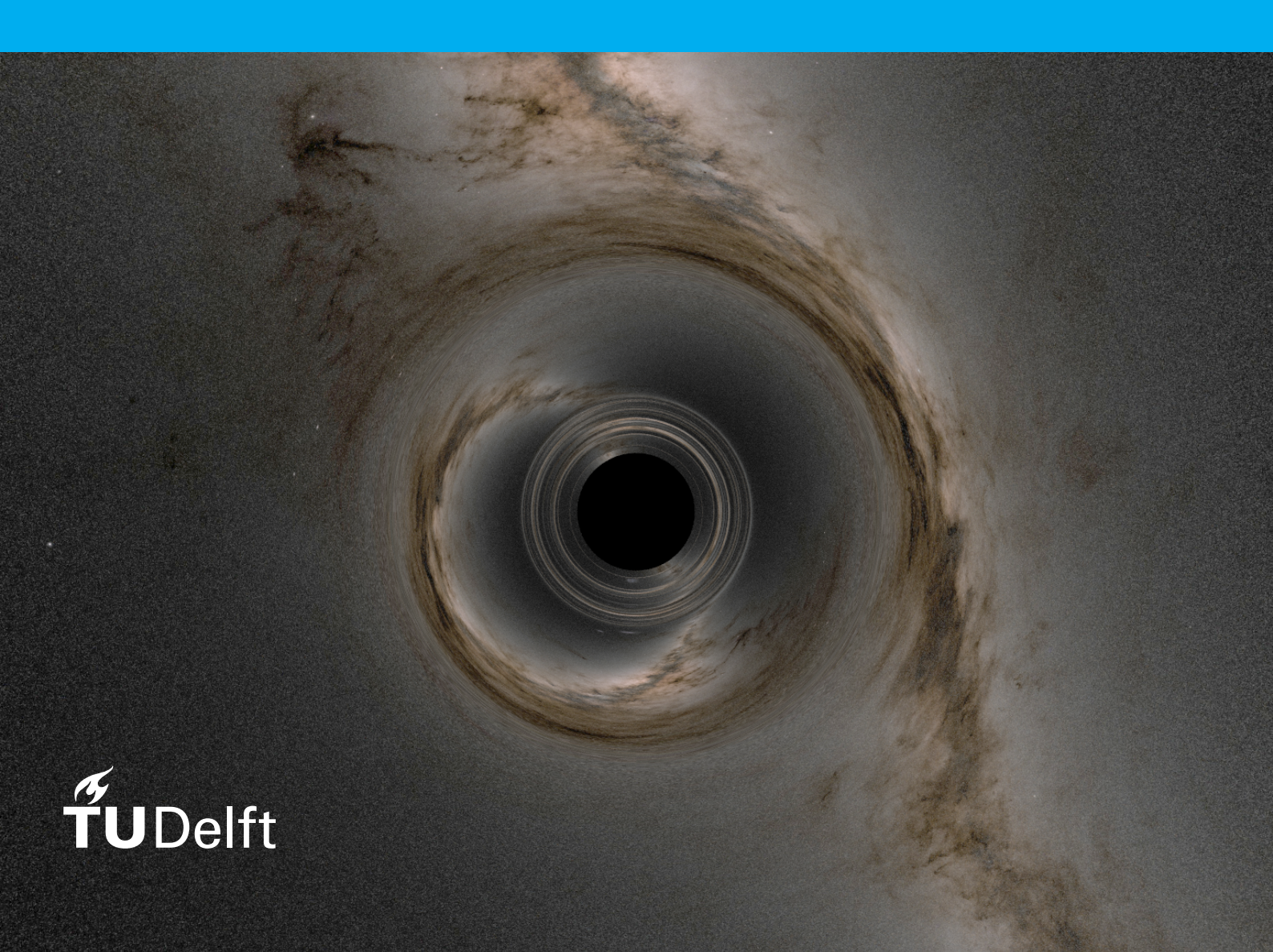
Imaging a Kerr Black Hole T.M. Kamminga

Bachelor Thesis Applied Mathematics

Supervisor
Dr. P.M. Visser
Advisor committee
Dr. K.P. Hart



Preface

The observations of the Event Horizon Telescope led to the first mages of a black hole, an object with so much gravity that not even light can escape it. These images remain fuzzy but clearly show the shadow of a black hole with a bright disk and will only improve in quality over time.

We want to be able to deduce, from the images, the following properties of the observed black hole; the mass, the angular momentum and the orientation of the black hole. This can be done by visualising the mathematical model of a black hole. This model is a result of the theory of general relativity and comparing the theoretical model to the real-life observations could be used to validate this theory.

We have visualized a Kerr black hole. This is a black hole that is more realistic than the original Schwarzschild black hole because it also includes the angular momentum of the black hole. The Kerr solution describes the curvature of space-time around a rotating black hole. This curvature of space-time causes light rays to travel in a curved path instead of a straight line. The distortion of light rays causes distortions in the image of a black hole in a similar way that a lens of a camera causes distortion in an image by curving light. By using the mathematical field of differential geometry we can exactly describe the curved path of a light ray around a Kerr black hole. This path of the light ray can be formulated in different coordinate systems. We will use the so-called Kerr-Schild coordinate system because it does not have the coordinate-related singularities of other coordinate systems.

To create the visualisation of a Kerr black hole we will implement a ray-tracing algorithm. This is an algorithm that can create a 2D projection of a 3D space. The algorithm normally uses straight light rays to create an image, we will however adapt this program to model the curved light rays around a Kerr black hole. The visualisation employs a celestial sphere around the black hole to project the universe around it. Furthermore, an accretion disk around the black hole is added to model light-emitting particles orbiting the black hole.

Our ray-tracing algorithm makes it possible to realistically visualise a Kerr black hole with varying parameters. These parameters are the mass of the black hole, the angular momentum, orientation compared to the observer and the size and structure of the accretion disk. To exemplify the ability of the ray-tracing model to fit these parameters, different angular momentum and orientation values are compared to the properties of the resulting image.

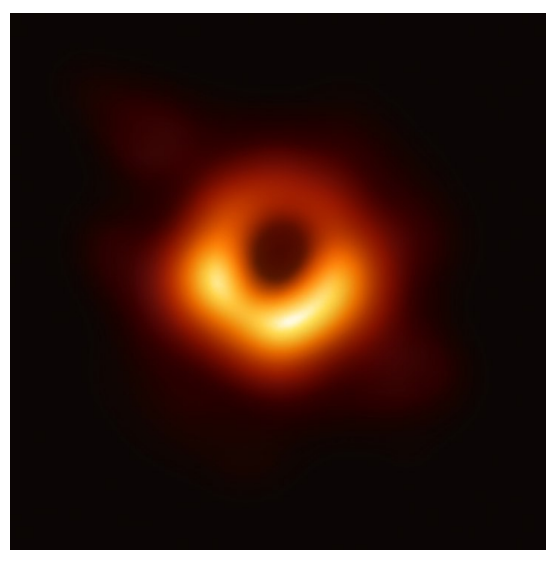
This means that when in the future we get higher resolution observations of a black hole, the properties of this black hole can be deduced from the ray-tracing model. This can help our understanding of the curvature of space-time caused by general relativity and our understanding of the universe as a whole.

T.M. Kamminga Delft, June 2022

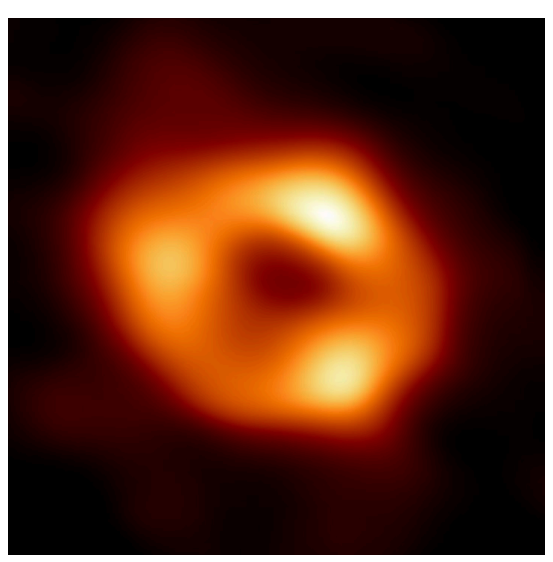
Contents

1	Introduction	1			
2	Differential geometry 2.1 Metric spaces. 2.2 Smooth manifolds 2.3 Einstein notation 2.4 Tangent spaces. 2.5 Riemann manifolds 2.6 Geodesics 2.7 Geodesics on the 2-sphere	3 5 5 6 8			
3	Geodesics in space-time 3.1 Minkowski space	12 12 14			
4	Ray tracing in curved space 4.1 Ray tracing	19			
5	Fitting the parameters of a Kerr black hole 2				
6	Conclusion	27			
Α	Code				

Introduction



(a) Messier 87*, a supermassive black hole with an estimated mass of $6 \cdot 10^9$ times the mass of the sun.



(b) Sagittarius A*, the supermassive black hole at the centre of the milky way with an estimated mass of $4 \cdot 10^6$ times the mass of the sun.

Figure 1.1: The first two images of a black hole, generated by the Event Horizon Telescope.

The first two images of a black hole have been released, of Messier 87* in 2019 visible in figure 1.1a and of Sagittarius A* in 2022 visible in figure 1.1b. These images remain fuzzy, but clearly show the shadow of a black hole in the middle of the image. They are both located at the centre of a galaxy and have masses of multiple magnitudes greater than the sun. But what is a black hole?

A black hole is an object with so much gravity that nothing can escape it. This means that even particles without mass like photons can not escape it. If you would look at the centre of a black hole there would be a black sphere emitting no light, explaining the name black hole. This sphere of no return surrounding the mass point has a radius called the Schwarzschild radius. The existence of black holes was first theorized before any observation. This was plausible because it is a result of Einstein's theory of general relativity. The main assumption of special relativity is that the speed of light can not be exceeded, in general relativity 4-dimensional space-time is curved which results in gravity. This curvature is also caused by the presence of mass. If this curvature is sufficient no particle can escape it and we end up with a black hole.

The theory of general relativity made many predictions which turned out to be true. It has also had many practical applications, such as more accurately determining your location with GPS, where time

dilation on GPS satellites has to be taken into account. Physics is however on an endless journey to check and expand its theories, so for general relativity we also want to do this. Near a black hole, the effects of relativity are the most severe and these objects thus are a great place to check the theory of general relativity in its most extreme environment.

Now that we have observations of black holes from the Event Horizon Telescope, can we use them to find the physical properties of these black holes? Three important parameters are mass, orientation and angular momentum of the black hole. A black hole is in a sense also a mathematical object, since it was at first a mathematical product of general relativity before any physical observation of it. A good place to start studying this object is by visualising it. The way to do this is by tracking the interaction of the black hole with the light hitting it and travelling in its surroundings. This light does not travel in a straight line because the space-time surrounding the black hole is curved.

Mathematics has a great tool set to study such curved spaces called differential geometry. The essential tools in this toolbox needed for modelling light in curved space-time will be defined chapter 2. Most important will be the concept of geodesics along which light rays travels. In chapter 3 we find the systems of differential equations which describe these geodesics for rotating and non-rotating black holes in different coordinate systems. After we have developed the mathematical know-how to model light around a black hole we can generate an image of it. This is done using ray tracing, where every pixel of an image is coloured using the path light would take to hit a virtual camera. This algorithm is further explained in chapter 4 starting at flat space and then expanding to curved space-time. Having developed the mathematics and the ray tracing algorithm, we can now generate images of black holes. This can be used to study black holes observed by astronomers. In chapter 5 an example of this is given by estimating the different parameters of a black hole based on a generated picture of it. Giving an amazing conclusion that you can study far-away black holes using only mathematics and a computer.

Before continuing on to the rest of the thesis I would like to thank Dr. P.M. Visser for his excellent support during the research en writing process. Without him the results would not be plausible. I would also like to thank Dr. K.P. Hart for joining the advisor committee.

Differential geometry

2.1. Metric spaces

Generating a simulated image of a black hole means that the paths of light through space-time curved by gravity have to be calculated. In normal day-to-day life we use Cartesian coordinates, often expressed as x, y and z coordinates. Furthermore, we calculate distances using the Pythagorean formula. This system is called the Euclidean space and is an example of a metric space. A metric space is defined as a non-empty set with a metric on the set. The metric is a distance function for this set defined as follows in Lay's book [5].

Definition 2.1.1. (Metric). Let X be any nonempty set. A function $d: X \times X \to \mathbb{R}$ is called a metric on X if it satisfies the following conditions for all $x, y, z \in X$.

- $(1) d(x, y) \ge 0$
- (2) d(x, y) = 0 if and only if x = y
- (3) d(x,y) = d(y,x)
- (4) $d(x,y) \le d(x,z) + d(z,y)$ (triangle inequality)

Example 2.1.1. Let $X = \mathbb{R} \times \mathbb{R} = \mathbb{R}^2$ and define $d : \mathbb{R}^2 \times \mathbb{R}^2 \to \mathbb{R}$ by

$$d((x_1, y_1), (x_2, y_2)) = \sqrt{(x_2 - x_1)^2 + (y_2 - y_1)^2}$$

for points (x_1, y_1) and (x_2, y_2) in \mathbb{R}^2

Example 2.1.2. Let X be a nonempty set and define d on X by

$$d(x,y) = \begin{cases} 0, & \text{if } x = y, \\ 1, & \text{if } x \neq y. \end{cases}$$

Example 2.1.1 is the Euclidean metric in \mathbb{R}^2 . This metric combined with the set \mathbb{R}^2 gives the Euclidean space in two dimensions, denoted by \mathbb{E}^2 . Example 2.1.2 gives the discrete metric, any nonempty set can be turned into a metric space using the discrete metric.

2.2. Smooth manifolds

As shown by example 2.1.2 metric spaces can be very general. Differential geometry studies more specific metric spaces called smooth manifolds. Bas Janssens in his course reader [4] roughly describes a smooth manifold as "a topological space that locally looks like \mathbb{R}^n ". The notion of a smooth manifold allows the use of differentiability in more general spaces than \mathbb{R}^n . The definition of a smooth manifold requires further concepts which will be given first. The definitions are from Bas Janssens's reader [4].

2.2. Smooth manifolds 4

Definition 2.2.1. (Hausdorff Spaces). A topological space M is called *Hausdorff* if for any two distinct points $x, y \in M$, there exist open neighbourhoods U_x of x and U_y of y which do not intersect, $U_x \cap U_y = \emptyset$.

Hausdorff spaces have the property that every sequence in the topological space has at most one limit. Spaces which are not Hausdorff will not be of interest to us.

Definition 2.2.2. (Chart). A *chart* on *M* is a homeomorphism

$$\phi: M \supseteq U \to \phi(U) \subseteq \mathbb{R}^n$$

from an open subset $U \subseteq M$ to an open subset $\phi(U) \subseteq \mathbb{R}^n$. U is the patch of the chart.

A chart can be seen as a coordinate transform from a specific set to \mathbb{R}^n

Definition 2.2.3. (Topological Atlas). Let $\mathcal{A} = \{(U_{\alpha}, \phi_{\alpha}); \alpha \in A\}$ be a collection of charts, labelled by an index set A. We say that \mathcal{A} is a *topological atlas* for M if M is the union of the coordinate patches $U_{\alpha}, M = \bigcup_{\alpha \in A} U_{\alpha}$.

A topological Atlas gives a coordinate transform for all points of the original set to \mathbb{R}^n

Definition 2.2.4. (Smooth Atlas). Let

$$\kappa_{\alpha\beta}:\phi_{\alpha}\left(U_{\alpha}\cap U_{\beta}\right)\to\phi_{\beta}\left(U_{\alpha}\cap U_{\beta}\right)$$

be defined by

$$\kappa_{\alpha\beta} := \phi_{\beta} \circ \phi_{\alpha}^{-1}.$$

Two charts $(U_{\alpha}, \phi_{\alpha})$ and $(U_{\beta}, \phi_{\beta})$ are called compatible if both $\kappa_{\alpha\beta}$ and $\kappa_{\beta\alpha}$ are smooth. A topological atlas \mathcal{A} is called smooth is all its charts are compatible.

This definition of two compatible charts means that if two different charts $(\phi_{\alpha}, U_{\alpha})$ and $(\phi_{\beta}, U_{\beta})$ describe the same function $f: M \to \mathbb{R}$ at p, they have to agree if f is smooth or not.

Definition 2.2.5. (Smooth manifold). A smooth manifold is a Hausdorff topological space M, together with a smooth atlas \mathcal{A} . We say that M is of dimension n if its charts take values in \mathbb{R}^n .

Example 2.2.1.

$$\mathbb{S}^2 := \{(x, y, z) \in \mathbb{R}^3; x^2 + y^2 + z^2 = 1\}$$

Example 2.2.1 is an example of a smooth manifold. \mathbb{S}^2 is the 2-sphere embedded in \mathbb{R}^3 and has dimension 2. Let n := (0,0,1) be the North Pole of the 2-sphere and s := (0,0,-1) the south pole. Then a possible chart for $\mathbb{S}^2 \setminus \{n\}$ is where the coordinates $(x,y) \in \mathbb{R}^2$ of a point $p = (\xi,\eta,\zeta)$ in \mathbb{S}^2 are

$$(x,y) = \left(\frac{\xi}{1-\zeta}, \frac{\eta}{1-\zeta}\right)$$

This is a projection in which every point p of the sphere is mapped to a point on the xy-plane which intersects the line, starting at p and passing through p. This projection is illustrated in figure 2.1. A projection for $\mathbb{S}^2 \setminus \{s\}$ is

$$(x,y) = \left(\frac{\xi}{1+\zeta}, \frac{\eta}{1+\zeta}\right)$$

This is the same projection as before just starting at the south pole. These two charts form a smooth atlas for \mathbb{S}^2 and \mathbb{S}^2 is a Hausdorff topological space. This means that \mathbb{S}^2 is a smooth manifold.

Now that we have defined a smooth manifold we can define differentiability in a smooth manifold. This will allow us to use calculus to solve problems in these spaces.

Definition 2.2.6. (Differentiable and smooth functions). A function $f: M \to \mathbb{R}$ is differentiable at $p \in M$ if for some chart U_{α} containing p, the coordinate representation $f \circ \phi_{\alpha}^{-1} : \mathbb{R}^n \supset \phi_{\alpha} (U_{\alpha}) \to \mathbb{R}$ is differentiable at $\phi_{\alpha}(p) \in \mathbb{R}^n$. Similarly, f is smooth at p if its coordinate representation is smooth at $\phi_{\alpha}(p)$.

2.3. Einstein notation 5

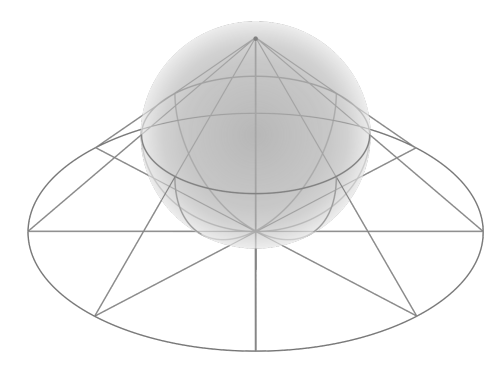


Figure 2.1: Stereographic projection of a 2-sphere to the *xy*-plane. Made by Mark Howison at English Wikipedia.

2.3. Einstein notation

Now that differentiation in a smooth manifold is introduced, we have the ability to do all kinds of calculus operations. This will often lead to long and cumbersome notation given a lot of partial differentials in different directions of the local unit vectors. To shorten the notation we will introduce the Einstein notation. In this notation summation over the indexes will be implied. This means that the vector $y \in \mathbb{R}^3$

$$y = \sum_{i=1}^{3} c_i x^i = c_1 x^1 + c_2 x^2 + c_3 x^3$$

is simplified in Einstein notation to:

$$y = c_i x^i$$

Where x^i represents a basis for \mathbb{R}^3 .

2.4. Tangent spaces

To study tangent spaces we will start with \mathbb{S}^2 given in example 2.2.1. Here we have the 2-dimensional smooth manifold embedded in \mathbb{R}^3 . For a point p on the sphere there exist multiple vectors such that these vectors are tangent to the surface in p. All these vectors form the tangent space. In this case, the tangent space is a plane. This tangent plane is illustrated in figure 2.2. If we define this tangent plane for every point we get the $\mathbb{S}^2 \times \mathbb{R}^2$ tangent bundle of \mathbb{S}^2 existing of all tangent vectors for every point on the sphere.

In this case, we embedded the two-dimensional sphere into the three-dimensional \mathbb{R}^3 . This meant that the tangent plane could leave the sphere as it lives in \mathbb{R}^3 . Most of the time we will not have the luxury of a manifold embedded in \mathbb{R}^n so we need to find a general definition for tangent spaces of a manifold. Bas Janssens gives the following definition for a tangent space which first requires an equivalence class:

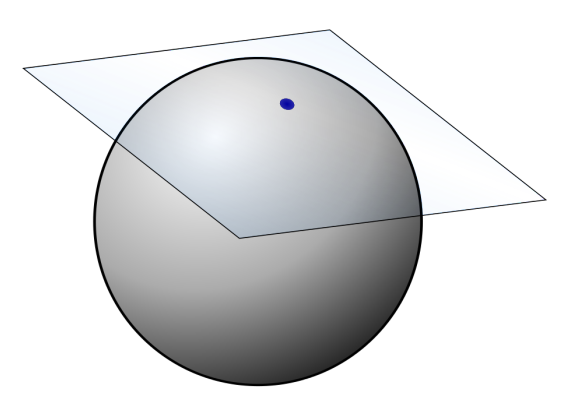


Figure 2.2: Tangent plane to point on the Sphere.

2.5. Riemann manifolds 6

Two curves γ and l that pass trough p are equivalent, $\gamma \sim_p l$, if there exists a chart (U_α,ϕ_α) around p in which the first order derivatives $v^\mu_\alpha = \dot{\gamma}^\mu_\alpha(0)$ and $w^\mu_\alpha = \dot{l}^\mu_\alpha(0)$ agree.

The μ in the superscript implies that all coordinate directions of the chart U_{α} must agree.

Definition 2.4.1. (Tangent space). A tangent vector at $p \in M$ is an equivalence class $v_p = [\gamma]$ of curves through p with respect to the relation \sim_p . The set T_pM of tangent vectors is called the tangent space of M at p.

A tangent vector van be tought of as the derivative of a curve $\gamma(t) \in [\gamma]$ when it passes trough p. So a vector $v \in T_p M$ can be written as $v = v^{\mu} \partial_{\mu}$, a linear combination of a basis ∂_{μ} of $T_p M$.

The ∂ sign comes from the fact that we use infinitely small basis vectors to represent the tangent space. Using the earlier example of a point p on the 2-sphere. There are no finitely sized tangent vectors of p on the sphere. But if we infinitely zoom in on the point p, the neighbourhood of p becomes flat and there are tangent vectors for p in this neighbourhood. This means that we have found infinitely small tangent vectors for p. The definition of a general tangent space is less intuitive than the more simple example of the plane tangent to the sphere, but the great improvement is that the smooth manifold does not have to be embedded in \mathbb{R}^n .

Now that we have defined tangent spaces we can also introduce tensors. A tensor is an algebraic object that allows us to do lots of calculations. The definition of a tensor is quite vague as the definition of a metric but can be defined for a manifold to make it more specific.

Definition 2.4.2. ((covariant) tensor). Let M be a manifold, and let p be a point in M. A (covariant) tensor of rank k at $p \in M$ is a multilinear map

$$\tau_p: \underbrace{T_pM \times ... \times T_pM}_{k \text{ times}} \to \mathbb{R}.$$

We will exclusively use tensors of rank 2, so bilinear maps: $T_pM \times T_pM \to \mathbb{R}$. A *tensor field* assigns a tensor to every point in a space.

2.5. Riemann manifolds

When we specified the notion of a smooth manifold we were able to use differentiability. But smooth manifolds still lack the concepts of distances and angles. So to constrain a space further we will introduce the concept of a Riemannian metric. This Riemannian metric differs from the Minkowski metric we will later use to study problems in space-time. We will however be able to introduce and study Geodesics which will be very important in the rest of this report. Bas Janssens [4] defines the Riemannian metric in the following way:

Definition 2.5.1. (Riemannian metric). A *Riemannian metric* g on M is a covariant tensor field of rank 2 such that for every point $p \in M$, the bilinear form $g_p : T_pM \times T_pM \to \mathbb{R}$ is an inner product.

For g_p to be an inner product it must be symmetric and $q_p(v,v)>0$ for all nonzero $v\in T_pM$. A Riemannian manifold is a smooth manifold equipped with a Riemannian metric. The most familiar Riemannian metric is the Euclidean space. The square of the Euclidean metric is equal to the dot product of two vectors in \mathbb{R}^n . The dot product is an example of an inner product. This implies that for all points $p\in\mathbb{R}^n$ the Euclidean metric g_p^E is Riemannian. This is illustrated in the language of tangent spaces by Janssens in example 2.5.1

Example 2.5.1. (Euclidean metric on \mathbb{R}^n). Let $M=\mathbb{R}^n$, and let x^1,\dots,x^n be the Cartesian coordinates on \mathbb{R}^n . This choice of local coordinates allows us to write $v,w\in T_p\mathbb{R}^n$ as $v=v^\mu\partial_\mu$ and $w=w^\mu\partial_\mu$. The Euclidean metric on $M=\mathbb{R}^n$ is given by

$$g_n^E \left(v^\mu \partial_\mu, w^\nu \partial_\nu \right) = v^1 w^1 + \dots + v^n w^n$$

We can now define any Riemannian metric on a smooth manifold as a matrix. For this, we will use the fact that for two points $v,w\in T_pM$ the metric must be a bilinear combination of the coordinates of v,w in a basis of T_pM . So for any x in the local coordinates of the chart of the manifold we have $g_p(v,w)=g_{\mu\nu}(x)v^\mu w^\nu$. We can now fill a matrix with all the different entries of $g_{\mu\nu}(x)$. This matrix G satisfies $g_p(v,w)=v^TGw$. This can be done for every tensor, the special feature of a Riemannian metric is that this matrix will be symmetric and positive.

2.5. Riemann manifolds 7

Example 2.5.2. (Euclidean matrix on \mathbb{R}^n) The Euclidean metric on \mathbb{R}^n has been given in example 2.5.1. The first thing we can see is that the metric is not dependent on the location x in \mathbb{R}^n . We further have $g^E_{\mu\nu}(x) = \delta_{\mu\nu}$. This means that the Euclidean matrix on \mathbb{R}^n is equal to the identity matrix I.

Example 2.5.3. (Euclidean metric on spherical coordinates) We start with the $M=\mathbb{R}^2$ and will then use the coordinate transfer to polar coordinates. So $x=r\cos(\phi)$ and $y=r\sin(\phi)$. This means that in the tangent space we have using the chain rule:

$$\partial_r = \frac{\partial x}{\partial r} \partial_x + \frac{\partial y}{\partial r} \partial_y = \cos(\phi) \partial_x + \sin(\phi) \partial_y$$
$$\partial_\phi = \frac{\partial x}{\partial \phi} \partial_x + \frac{\partial y}{\partial \phi} \partial_y = -r \sin(\phi) \partial_x + r \cos(\phi) \partial_y$$

This allows us to quickly calculate all tensors using the Euclidean metric. We will use that $g_{r\phi}=g_{\phi r}$ because the Euclidean metric is symmetric.

$$g_{rr} = g(\partial_r, \partial_r) = \cos^2(\phi) + \sin^2(\phi) = 1$$

$$g_{\phi\phi} = g(\partial_\phi, \partial_\phi) = -r^2 \sin^2(\phi) + r^2 \cos^2(\phi) = r^2$$

$$g_{r\phi} = g_{\phi r} = g(\partial_\phi, \partial_r) = -r \cos(\phi) \sin(\phi) + r \cos(\phi) \sin(\phi) = 0$$

So this results in the following matrix:

$$\begin{pmatrix} g_{rr} & g_{r\phi} \\ g_{\phi r} & g_{\phi \phi} \end{pmatrix} = \begin{pmatrix} 1 & 0 \\ 0 & r^2 \end{pmatrix}$$

Now that the Riemannian metric is introduced we can have a definition of distance. If we think back to the example of the 2-sphere embedded in \mathbb{R}^3 , any vector between two different points on the sphere leaves the sphere. So measuring distances this way does not make sense in the 2-sphere. We will begin by defining distances for the infinitesimally small vectors in the tangent space T_pM of a point p in a smooth manifold M.

Definition 2.5.2. (Length tangent space). If (M, g) is a Riemannian manifold, then the *length* of $v \in T_pM$ is defined as

$$||v|| := \sqrt{g_p(v, v)}$$

Now that we have defined the length of a vector in the tangent space we can "stitch" all these lengths together by integration to get the length of a piecewise regular curve in a smooth manifold.

Definition 2.5.3. (Length curve). Let $[a, b] \subseteq \mathbb{R}$ be a closed interval. Then the piecewise regular curve $\gamma : [a, b] \to M$ on a Riemannian manifold (M, g) has *length* defined by

$$\mathcal{L}(\gamma) := \int_{a}^{b} \|\dot{\gamma}(t)\| dt$$

A curve is *regular* if it is smooth and $\dot{\gamma}(t) \neq 0$ for all $t \in [a, b]$. A curve is *piecewise regular* if a finite closed subdivision of the curve is regular.

Example 2.5.4. (length equator 2-sphere) Let \mathbb{S}_r^2 be the 2-sphere with radius r embedded in \mathbb{R}^3 . We will use the Euclidean metric. The path around the equator can be parameterised by the function $\gamma:[0,2\pi]\to\mathbb{S}_r^2$ given by

$$\gamma(t) := (r\cos(t), r\sin(t), 0)$$

This gives a length

$$\mathcal{L}(\gamma) = \int_0^{2\pi} \|\dot{\gamma}(t)\| \, dt = \int_0^{2\pi} \|(-r\sin(t), r\cos(t), 0)\| \, dt$$
$$= \int_0^{2\pi} \sqrt{r^2(\cos^2(t) + \sin^2(t))} \, dt = 2\pi \cdot r$$

2.6. Geodesics 8

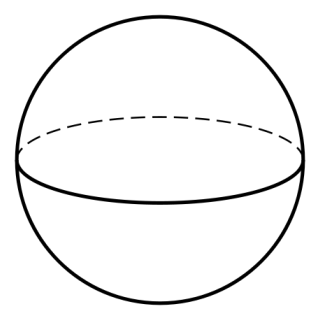


Figure 2.3: The equator of a sphere

Which is the size of the equator of a sphere with radius r, as illustrated in figure 2.3. The only thing left to define before we can continue to geodesics is a distance function between two points. This is quite straightforwardly defined as the infimum of the length of all curves between the two points.

Definition 2.5.4. (Distance). The distance d(p,q) between two points p and q on M is defined as

$$d(p,q) := \inf\{\mathcal{L}(\gamma); \gamma(\alpha) = p \text{ and } \gamma(b) = q\}$$

where the infimum is taken over all piecewise regular curves $\gamma:[a,b]\to M$ that start at p and end at q.

2.6. Geodesics

In non-curved flat space straight lines exist and give the shortest path possible between two points. In curved spaces "straight lines" do not always exist. We can think of walking over the earth's surface, if we walk between two cities we can never walk in an exact straight line. The path we would walk has some curvature because the earth is not flat. We would like to generalise the concept of a "straight line" to curved surfaces such that we can still find the shortest path between two points. This can be done by a geodesic, which can be thought of as the most straight-line plausible. Bas Janssens [4] gives the following definition for a geodesic, where regular means that it's derivative never vanishes.

Definition 2.6.1. (Geodesics). A geodesic on M is a piecewise regular curve $\gamma:[a,b]\to M$ with unit speed $||\dot{\gamma}(t)||=1$, such that for all $t_0\in[a,b]$, there exists an open interval $I\subseteq[a,b]$ around t_0 with

$$d\left(\gamma(t),\gamma\left(t'\right)\right) = |t - t'|$$

for all $t, t' \in I$.

On \mathbb{R}^n all geodesics are straight lines as shown in example 2.6.1, but if the space is curved the geodesic can have other forms. Figure 2.3 illustrates a geodesic on the 2-sphere, which we prove in section 2.7 are all great circles. Further examples in different curved spaces will be given in the next chapter.

Definition 2.6.1 is a very elegant and compact definition for a geodesic we would, however, like to have an alternative way to find geodesics using differential equations. This will allow us to numerically approximate geodesics in the future. Theorem 2.6.1 gives us these differential equations. The proof for this theorem is available in the reader by Bas Janssens [4].

Theorem 2.6.1. (Geodesic equation). Every geodesic is regular. In local coordinates, it satisfies the second-order ODE

$$\ddot{\gamma}^{\mu} + \Gamma^{\mu}_{\sigma\tau} \dot{\gamma}^{\sigma} \dot{\gamma}^{\tau} = 0$$

with the so-called Christoffel symbols $\Gamma^{\mu}_{\sigma\tau}$ given by

$$\Gamma^{\mu}_{\sigma\tau} = \frac{1}{2} g^{\mu\alpha} \left(\partial_{\sigma} g_{\tau\alpha} + \partial_{\tau} g_{\alpha\sigma} - \partial_{\alpha} g_{\sigma\tau} \right)$$

Where $g^{\mu\alpha}$ are the elements of the inverse matrix of $g_{\mu\alpha}$. So if we use the matrix of example 2.5.3 we get.

$$\begin{pmatrix} g^{rr} & g^{r\phi} \\ g^{\phi r} & g^{\phi \phi} \end{pmatrix} = \begin{pmatrix} g_{rr} & g_{r\phi} \\ g_{\phi r} & g_{\phi \phi} \end{pmatrix}^{-1}$$

If a manifold has n dimensions there are n^3 Christoffel symbols. Example 2.6.1 shows that all geodesics in Euclidean space are straight lines. Many more examples of the applications of the geodesic equations in curved spaces will be given in the next chapter.

Example 2.6.1. (Geodesics in Euclidian space) From example 2.5.2 we know that in \mathbb{E}^n $g_{\mu\nu}=\delta_{\mu\nu}$. So any partial derivative of the metric is 0. This implies

$$\Gamma^{\mu}_{\sigma\tau} = \frac{1}{2} g^{\mu\alpha} \left(\partial_{\sigma} g_{\tau\alpha} + \partial_{\tau} g_{\alpha\sigma} - \partial_{\alpha} g_{\sigma\tau} \right)$$
$$= \frac{1}{2} g^{\mu\alpha} (0 + 0 - 0)$$
$$= 0$$

By the geodesic equation, we have that all geodesics □have the property

$$\ddot{\gamma}^{\mu} = 0$$

So all geodesics are linear curves in \mathbb{E}^n .

2.7. Geodesics on the 2-sphere

For an example of non-straight geodesic will look at the example of the 2-sphere. In example 2.2.1 we defined the 2-sphere \mathbb{S}^2 in the following way.

$$\mathbb{S}^2 := \{(x, y, z) \in \mathbb{R}^3; x^2 + y^2 + z^2 = 1\}$$

We can use the following parameterization for the 2-sphere embedded in \mathbb{R}^n .

$$x = \cos \phi \sin \theta$$
, $y = \sin \phi \sin \theta$, $z = \cos \theta$

The chain rule then gives us the following basis for the tangent space.

$$\begin{aligned} \partial_{\theta} &= \frac{\partial x}{\partial \theta} \partial_{x} + \frac{\partial y}{\partial \theta} \partial_{y} + \frac{\partial z}{\partial \theta} \partial_{z} \\ &= \cos \phi \cos \theta \, \partial_{x} + \sin \phi \cos \theta \, \partial_{y} + \sin \theta \, \partial_{z} \\ \partial_{\phi} &= \frac{\partial x}{\partial \phi} \partial_{x} + \frac{\partial y}{\partial \phi} \partial_{y} + \frac{\partial z}{\partial \phi} \partial_{z} \\ &= -\sin \phi \sin \theta \, \partial_{x} + \cos \phi \sin \theta \, \partial_{y} \end{aligned}$$

Taking the inner products we can now calculate the tensors.

$$g_{\theta\theta} = \cos^2\phi \cos^2\theta + \sin^2\phi \cos^2\theta + \sin^2\theta = 1$$

$$g_{\theta\phi} = g_{\phi\theta} = -\sin\phi \cos\phi \cos\theta \sin\theta + \sin\phi \cos\phi \cos\theta \sin\theta = 0$$

$$g_{\phi\phi} = \sin^2\theta \sin^2\phi + \sin^2\theta \cos^2\phi = \sin^2\theta$$

So we end up with the following matrix and inverse matrix for the tensors.

$$\begin{pmatrix} g_{\theta\theta} & g_{\theta\phi} \\ g_{\phi\theta} & g_{\phi\phi} \end{pmatrix} = \begin{pmatrix} 1 & 0 \\ 0 & \sin^2 \theta \end{pmatrix}$$
$$\begin{pmatrix} g^{\theta\theta} & g^{\theta\phi} \\ g^{\phi\theta} & g^{\phi\phi} \end{pmatrix} = \begin{pmatrix} g_{\theta\theta} & g_{\theta\phi} \\ g_{\phi\theta} & g_{\phi\phi} \end{pmatrix}^{-1} = \begin{pmatrix} 1 & 0 \\ 0 & \sin^{-2} \theta \end{pmatrix}$$

Now we can calculate the Christoffel symbols $\Gamma^{\mu}_{\sigma\tau}$ using the following formula.

$$\Gamma^{\mu}_{\sigma\tau} = \frac{1}{2} g^{\mu\alpha} \left(\partial_{\sigma} g_{\tau\alpha} + \partial_{\tau} g_{\alpha\sigma} - \partial_{\alpha} g_{\sigma\tau} \right)$$

As θ is the only variable in the tensors we get that $\partial_{\theta} g_{\phi\phi}$ is the only nonzero partial derivative in the formula of the Christoffel symbols. We can also use that $\Gamma^{\mu}_{\sigma\tau} = \Gamma^{\mu}_{\tau\sigma}$ because of the symmetry of the tensors. So all nonzero Christoffel symbols are:

$$\Gamma^{\phi}_{\theta\phi} = \Gamma^{\phi}_{\phi\theta} = \frac{1}{2} g^{\phi\phi} \partial_{\theta} g_{\phi\phi} = \frac{1}{2} \sin^{-2} \theta \cdot 2 \sin \theta \cos \theta = \frac{\cos \theta}{\sin \theta}$$
$$\Gamma^{\theta}_{\phi\phi} = -\frac{1}{2} g^{\theta\theta} \partial_{\theta} g_{\phi\phi} = -\frac{1}{2} \cdot 2 \sin \theta \cos \theta = -\sin \theta \cos \theta$$

So by the geodesic equation of theorem 2.6.1 we get that any geodesic γ on the unit sphere must adhere to the following differential equations.

$$\ddot{\gamma}^{\phi} + 2 \cdot \Gamma^{\phi}_{\theta\phi} \dot{\gamma}^{\theta} \dot{\gamma}^{\phi} = 0$$
$$\ddot{\gamma}^{\theta} + \Gamma^{\theta}_{\phi\phi} \dot{\gamma}^{\theta} \dot{\gamma}^{\theta} = 0$$

Which gives

$$\ddot{y}^{\phi} + 2 \frac{\cos \theta}{\sin \theta} \dot{y}^{\theta} \dot{y}^{\phi} = 0$$
$$\ddot{y}^{\theta} - \sin \theta \cos \theta \dot{y}^{\theta} \dot{y}^{\theta} = 0$$

A simple curve on \mathbb{S}^2 that is a solution of these differential equations is the great circle on the unit sphere from example 2.5.4. This great circle is parameterized in the following way.

$$\gamma(t) := (\cos(t), \sin(t), 0)$$

In spherical coordinates this curve is described as

$$(\phi(t), \theta(t)) = (t, \frac{\pi}{2})$$

We get that $\ddot{\gamma}^{\phi} = \ddot{\gamma}^{\theta} = \dot{\gamma}^{\theta} = 0$ so this curve is a solution to the previous system of differential equations. We can use the symmetry of the sphere and the indifference of the orientation of the coordinate transfer to conclude that all great circles on the sphere must be geodesics.

Geodesics in space-time

3.1. Minkowski space

In previous examples, we only looked at spatial dimensions but the Einstein's relativity uses the concept of space-time. This means we will have 3 spatial dimensions and a special time dimension. These dimensions are combined using the Minkowski metric. This metric η treats time different than the spatial dimensions and is given by

$$\eta(v, w) := -v_0 w_0 + v_1 w_1 + v_2 w_2 + v_3 w_3$$

The Minkowski space \mathbb{M}^4 is defined as the set \mathbb{R}^4 with the Minkowski metric η . η is not actually a metric by definition 2.1.1 because we can have $\eta(v,w) \leq 0$ and $\eta(v,w) = 0$ for $v \neq w$. We will however call it a metric from now on. A big assumption in Einstein's relativity is that the speed of light can not be exceeded. This can be seen as a limit on the Minkowski metric. Assume a particle travels at a speed less than or equal to the speed of light. Let $p,q \in \mathbb{M}^4$ and $\Delta x, \Delta y, \Delta z$ be the distance traveled from p to q in the x,y and z direction respectively. Assume the time difference Δt is positive. The speed limit implies

$$\frac{\sqrt{\Delta x^2 + \Delta y^2 + \Delta z^2}}{\Delta t} \le c$$
$$\frac{\Delta x^2 + \Delta y^2 + \Delta z^2}{\Delta t^2} \le c^2$$
$$\Delta x^2 + \Delta y^2 + \Delta z^2 - \Delta t^2 c^2 \le 0$$

We can choose the units such that c=1 for example by using seconds for the time and distances. So for an observer in the present place p, a future event q must have $\eta(q-p,q-p)\leq 0$. If a particle travels without acceleration at the speed of light we must have $\eta(q-p,q-p)=0$. The limit on the speed of a particle can be seen as a restriction such that all future events in space-time must be in a 4D cone with radius $c\Delta t$. If we only allow for 2 spatial dimensions the cone becomes three-dimensional and is easier to visualise. This cone can be seen in figure 3.1. There is a cone for future and past events. If a particle travels with the speed of light it must be on these cones otherwise, it has to be inside these cones.

We can write the metric $\eta(v, w)$ in matrix form as

$$\eta(v,w) = v^{\mathsf{T}} \begin{pmatrix} -1 & 0 & 0 & 0 \\ 0 & 1 & 0 & 0 \\ 0 & 0 & 1 & 0 \\ 0 & 0 & 0 & 1 \end{pmatrix} w$$

Since there are no variables in this tensor matrix we can conclude that all Christoffel symbols are equal to 0. From theorem 2.6.1 we thus get that all straight lines are geodesics in \mathbb{M}^4 . This will include curves representing particles going faster than light these can be filtered out by the additional constraint $\eta \leq 0$.

3.2. Lorentzian manifolds 12

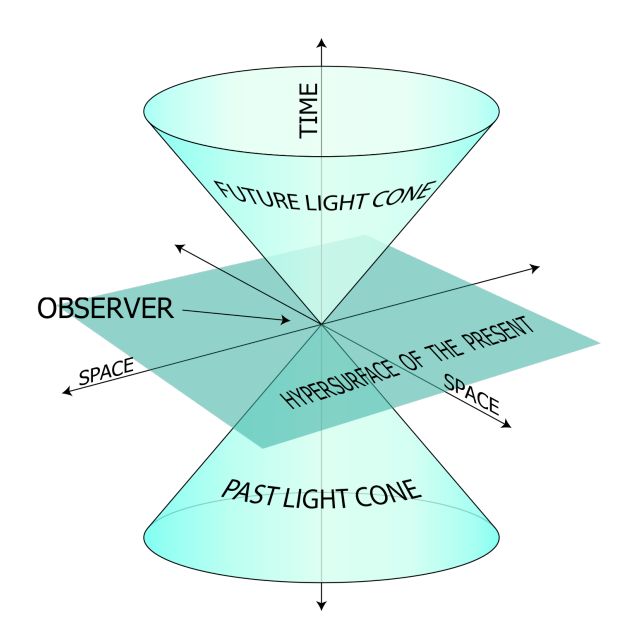


Figure 3.1: Past and future light cone

3.2. Lorentzian manifolds

In section 2.5 we defined a Riemannian metric as an inner product $g_p:T_pM\times T_pM\to\mathbb{R}$. For a Lorentzian metric we drop the positive definite assumption of the inner product but add a new assumption; at point p there must be a basis $e^0(p), e^1(p), e^2(p), e^3(p)$ of T_pM such that $g_p(e_0, e_0) = -1$, $g_p(e_i, e_i) = 1$ for i=1,2,3 and $g_p(e_i,e_j)=0$ for $j\neq i$. A Lorentzian manifold is a manifold with a Lorentzian metric. For a Riemannian manifold it was the case that the infinitely small tangent space T_pM around p had the structure of an Euclidean space. The tangent space T_pM around p in a Lorentzian manifold has the structure of a Minkowski space. This allows us to make calculations in curved space-time. Because a Lorentz manifold is an generalisation of a Riemannian manifold it is called a pseudo-Riemannian manifold.

Definition 2.6.1 of a geodesic does not make sense in a Lorentzian manifold because the condition of unit speed $\|\dot{\gamma}(t)\| = 1$ for a curve γ is not plausible with the Minkowski metric. There however still exists a similar definition that still leads to the same geodesic equation of theorem 2.6.1. This is the equation we will use to find geodesics in Lorentzian manifolds. namely

$$\ddot{\gamma}^{\mu} + \Gamma^{\mu}_{\sigma\tau} \dot{\gamma}^{\sigma} \dot{\gamma}^{\tau} = 0$$

3.3. Schwarzschild solution

In 1915 Einstein published the Einstein field equations. These formulas describe the curvature of space-time by gravitation. In the same year, Karl Schwarzschild found a solution to the field equations for a non-rotation non-charged spherical mass. This is the most simple example of space-time deformed by gravitation. The solution is given by the Schwarzschild metric in spherical coordinates taken from the Encyclopedia of Mathematical Physics [3]. Using natural units means we can take the gravitational constant G=1.

$$ds^{2} = -\left(1 - \frac{2M}{r}\right)dt^{2} + \left(1 - \frac{2M}{r}\right)^{-1}dr^{2} + r^{2}\left(d\theta^{2} + \sin^{2}\theta d\varphi^{2}\right)$$

Where θ , ϕ and r are the spherical coordinates with a spherical mass at the center. The spherical object at r=0 has mass M. Equivalently the metric can be written in matrix form using the formula

 $ds^2 = g_{\alpha\beta} dx^\alpha dx^\beta.$

$$\begin{pmatrix} g_{tt} & g_{tr} & g_{t\theta} & g_{t\phi} \\ g_{rt} & g_{rr} & g_{r\theta} & g_{r\phi} \\ g_{\theta t} & g_{\theta r} & g_{\theta \theta} & g_{\theta \phi} \\ g_{\phi t} & g_{\phi r} & g_{\phi \theta} & g_{\phi \phi} \end{pmatrix} = \begin{pmatrix} -1 + \frac{2M}{r} & 0 & 0 & 0 \\ 0 & \frac{1}{1 - \frac{2M}{r}} & 0 & 0 \\ 0 & 0 & r^2 & 0 \\ 0 & 0 & 0 & r^2 \sin[\theta]^2 \end{pmatrix}$$

To find the paths of light rays in the Schwarzschild solution the Christoffel symbols of theorem 2.6.1 again need to be calculated. This can be done by hand, but this is a long and error-prone problem, especially in the next parts of this chapter where the complexity of the metric will increase. So instead we will calculate these Christoffel symbols using the symbolic computation program Wolfram Mathematica. This will allow us to insert an arbitrary metric and get the resulting Christoffel symbols and geodesic equation. The code to calculate the Christoffel symbols and geodesic equation is adapted from a paper by Erik Tollerud [9]. The function used to calculate a Christoffel symbol from a metric and an inverse metric is given below. It is the Mathematica interpretation of the definition of a Christoffel symbol from 2.6.1.

```
\begin{aligned} & \text{christ}[a\_,b\_,c\_]\text{:=christ}[a,b,c] = \\ & \text{Simplify}\left[\sum_{d=1}^4 (1/2) \text{inversemetric}[[a,d]](\\ & D[\text{metric}[[d,c]], \text{coord}[[b]]] \\ & + D[\text{metric}[[d,b]], \text{coord}[[c]]] \\ & - D[\text{metric}[[b,c]], \text{coord}[[d]]])]] \end{aligned}
```

"metric" and "inversemetric" are the metric matrix and the inverse metric matrix respectively, "coord" is the list with coordinates $\{t, x, y, z\}$. This gives the following non-zero Christoffel symbols for the Schwarzschild metric.

$$\Gamma_{tr}^{t} = \Gamma_{rt}^{t} = -\frac{M}{2Mr - r^{2}}$$

$$\Gamma_{r\theta}^{\theta} = \Gamma_{\theta r}^{\theta} = \frac{1}{r}$$

$$\Gamma_{rr}^{r} = \frac{M(r - 2M)}{r^{3}}$$

$$\Gamma_{rr}^{\theta} = \Gamma_{\theta r}^{\theta} = \frac{1}{r}$$

$$\Gamma_{rr}^{\phi} = \Gamma_{r\phi}^{\phi} = \frac{1}{r}$$

$$\Gamma_{\theta \theta}^{\phi} = \Gamma_{r\phi}^{\phi} = \cot(\theta)$$

$$\Gamma_{\theta \phi}^{r} = \sin^{2}(\theta)(2M - r)$$

$$\Gamma_{\theta \phi}^{\theta} = \sin(\theta)(-\cos(\theta))$$

We can now use these Christoffel symbols and theorem 2.6.1 to calculate the differential equations for the geodesics for the Schwarzschild solution. The following piece of code is the translation of the geodesic equation in Mathematica.

```
\begin{split} & \text{geodesic:=} \\ & \text{geodesic} = \\ & \text{Simplify[Table[} \\ & - \text{Sum[christ}[i,j,k] \text{coord}[[j]]' \text{coord}[[k]]', \{j,1,n\}, \{k,1,n\}], \{i,1,n\}]] \end{split}
```

Where christ is the previously defined function and coord[[j]]' represents the derivative of the coordinate in the coordinate list coord. This results in the following system of differential equations.

$$\ddot{t} = \frac{2M\dot{r}\dot{t}}{2Mr - r^2}$$

$$\ddot{r} = \frac{(r - 2M)^2 \left(M\dot{t}^2 - r^3 \left(\dot{\theta}^2 + \sin^2(\theta)\dot{\phi}^2\right)\right) - Mr^2\dot{r}^2}{r^3 (2M - r)}$$

$$\ddot{\theta} = \sin(\theta)\cos(\theta)\dot{\phi}^2 - \frac{2\dot{\theta}\dot{r}}{r}$$

$$\ddot{\phi} = -\frac{2\dot{\phi}\left(\dot{r} + r\dot{\theta}\cot(\theta)\right)}{r}$$

3.4. Schwarzschild solution in Kerr-Schild Cartesian

In 1963 Roy Kerr expanded the Schwarzschild metric to add rotational momentum to the model. In the original Schwarzschild model the mass is centred at a single point so has no angular momentum. However when black holes collapse they are generally rotating so this angular momentum is retained. This means that Kerr's solution is more realistic. If we set the angular momentum to be 0 in Kerr's solution we end back up at the Schwarzschild case. The Kerr solution has different geometrical forms, one of which is in Cartesian coordinates. This solution is called Kerr–Schild "Cartesian". The Kerr-Schild metric with no angular momentum in Cartesian coordinates is given by Matt Visser [10] as

$$ds^{2} = -dt^{2} + dx^{2} + dy^{2} + dz^{2} + \frac{2M}{r} \left(dt + \frac{x dx + y dy + z dz}{r} \right)^{2}$$

where

$$r = \sqrt{x^2 + y^2 + z^2}$$

When m=0 this metric returns to the Minkowski metric. This solution has several advantages compared to the Schwarzschild solution of part 3.3. One advantage is that the gravitational curvature is given by only the last element. This means that an approximation could be made of a situation where there are more than one mass point in the simulation. Another advantage is there is no singularity along the z-axis because of the Cartesian coordinates instead of the spherical coordinates. A further advantage is that the solution is still stable inside the Schwarzschild radius. In the real world, the volume inside of this radius is not relevant but the model should give no problems if a simulated light ray enters this sphere because of numerical errors. Near r=0 these problems will still occur, but this is unavoidable. In matrix form, the metric can be written as

$$\begin{pmatrix} g_{tt} & g_{tx} & g_{ty} & g_{tz} \\ g_{xt} & g_{xx} & g_{xy} & g_{xz} \\ g_{yt} & g_{yx} & g_{yy} & g_{yz} \\ g_{zt} & g_{zx} & g_{zy} & g_{zz} \end{pmatrix} = \begin{pmatrix} \frac{2M}{r} - 1 & \frac{2Mx}{r^2} & \frac{2My}{r^2} & \frac{2Mz}{r^2} \\ \frac{2Mx}{r^2} & \frac{2Mx^2}{r^3} + 1 & \frac{2Mxy}{r^3} & \frac{2Mxz}{r^3} \\ \frac{2My}{r^2} & \frac{2Mxy}{r^3} & \frac{2My^2}{r^3} + 1 & \frac{2Myz}{r^3} \\ \frac{2Mz}{r^2} & \frac{2Mz}{r^3} & \frac{2Mz}{r^3} & \frac{2Mz}{r^3} + 1 \end{pmatrix}$$

What stands out is that this is not a diagonal matrix like previous tensor matrices of the metric. This is because the curved space is not symmetric in the Cartesian coordinates. The fact that the matrix is not diagonal adds two complexities to calculating the ODE for the geodesic. The first is that finding the inverse of the matrix is not as trivial as with a diagonal matrix, where the individual element of the matrix can be inverted. However because the last non-Minkowski part of the metric forms a null vector this inverse can still be written in the nice form

$$-\partial t^2 + \partial x^2 + \partial y^2 + \partial z^2 - \frac{2M}{r} \left(-\partial t + \frac{x\partial x + y\partial y + z\partial z}{r} \right)^2$$

The second complexity is that since more tensors are nonzero, more Christoffel symbols will be nonzero and the complexity of the differential equation will increase. However by letting Mathematica do the

algebraic work this inconvenience is mostly overcome. Reusing the geodesic function of part ,3.3 we get the following ODE

$$\ddot{t} = \frac{2M(\dot{y}^2(r^3 - y^2(M + 2r)) + \dot{z}^2(r^3 - z^2(M + 2r)) - Mr^2\dot{t}^2 + \dot{x}^2(r(r^2 - 2x^2) - Mx^2) - r\dot{t}(2M + r)(x\dot{x} + y\dot{y} + z\dot{z}) - 2x\dot{x}(M + 2r)(y\dot{y} + z\dot{z}) - 2y\dot{y}z\dot{z}(M + 2r))}{r^5}$$

$$\ddot{x} = \frac{Mx(\dot{x}^2(x^2(2M + 3r) - 2r^3) + r^2\dot{t}^2(2M - r) + \dot{z}^2(z^2(2M + r) - 2r(r^2 - z^2)) + 4Mr\dot{t}(x\dot{x} + y\dot{y} + z\dot{z}) + y^2(2My^2 + r(-2x^2 + y^2 - 2z^2)) + 2x\dot{x}(2M + 3r)(y\dot{y} + z\dot{z}) + 2y\dot{y}z\dot{z}(2M + 3r))}{r^6}$$

$$\ddot{y} = \frac{My(\dot{x}^2(x^2(2M + 3r) - 2r^3) + r^2\dot{t}^2(2M - r) + \dot{z}^2(z^2(2M + r) - 2r(r^2 - z^2)) + 4Mr\dot{t}(x\dot{x} + y\dot{y} + z\dot{z}) + y^2(2My^2 + r(-2x^2 + y^2 - 2z^2)) + 2x\dot{x}(2M + 3r)(y\dot{y} + z\dot{z}) + 2y\dot{y}z\dot{z}(2M + 3r))}{r^6}$$

$$\ddot{z} = \frac{Mz(\dot{x}^2(x^2(2M + 3r) - 2r^3) + r^2\dot{t}^2(2M - r) + \dot{z}^2(z^2(2M + r) - 2r(r^2 - z^2)) + 4Mr\dot{t}(x\dot{x} + y\dot{y} + z\dot{z}) + y^2(2My^2 + r(-2x^2 + y^2 - 2z^2)) + 2x\dot{x}(2M + 3r)(y\dot{y} + z\dot{z}) + 2y\dot{y}z\dot{z}(2M + 3r)}{r^6}$$

3.5. Kerr solution in Kerr-Schild coordinates

As mentioned in paragraph 3.4 Roy Kerr discovered the solution to the Einstein equations for a spinning black hole. This solution, just like the Schwarzschild solution has many coordinate forms. One of the most common ones is the solution in Boyer–Lindquist coordinates. The Boyer–Lindquist coordinates are oblate spheroidal coordinates, a generalisation of spherical coordinates where for a given radius you get an oblate spheroid instead of a sphere. So the 2D equivalent is elliptical coordinates instead of polar coordinates. This solution uses the "shape" of the spinning black hole to make the metric as simple as possible resulting in only two non-diagonal elements in the metric matrix giving more zero Christoffel symbols and a shorter geodesic equation. This coordinate system just like the Schwarzschild solution of paragraph 3.3 has mathematical singularities on the *z*-axis which leads to big numerical errors in the ray tracing process as seen in the image generated by Raquepas and Schulz [6] in figure 3.2. One solution is to use another numerical method near the poles as in Chan's webinar [1].



Figure 3.2: Singularity in the z-axis as a result of using the Boyer–Lindquist coordinates. Where the image is generated by Renaud and Schulz [6].

The more general solution to this problem is to use Kerr-Schild coordinates, which are well behaved on the z-axis and only have a singularity at the centre of the black hole. This is the approach used in this thesis. The Kerr-metric in Kerr-Schild coordinates is given as [10]

$$\begin{split} \mathrm{d}s^2 &= -\,\mathrm{d}t^2 + \mathrm{d}x^2 + \mathrm{d}y^2 + \mathrm{d}z^2 \\ &+ \frac{2mr^3}{r^4 + a^2z^2} \left(\,\mathrm{d}t + \frac{r(x\;\mathrm{d}x + y\;\mathrm{d}y)}{a^2 + r^2} + \frac{a(y\;\mathrm{d}x - x\;\mathrm{d}y)}{a^2 + r^2} + \frac{z}{r}\;\mathrm{d}z\right)^2 \end{split}$$

with

$$R^{2} = x^{2} + y^{2} + z^{2}$$

$$r = \sqrt{\frac{R^{2} - a^{2} + \sqrt{(R^{2} - a^{2})^{2} + 4a^{2}z^{2}}}{2}}$$

Where a is the rotational parameter that can vary between 0 and M. As $a \to 0$, we get the Schwarzschild case of paragraph and if also $M \to 0$ we get the Minkowski case. In matrix form, we write the metric as

$$\begin{pmatrix} g_{tt} & g_{tx} & g_{ty} & g_{tz} \\ g_{xt} & g_{xx} & g_{xy} & g_{xz} \\ g_{yt} & g_{yx} & g_{yy} & g_{yz} \\ g_{zt} & g_{zx} & g_{zy} & g_{zz} \end{pmatrix} = \\ \begin{pmatrix} \frac{2Mr^3}{a^2z^2+r^4} - 1 & \frac{2Mr^3(ay+rx)}{(a^2+r^2)(a^2z^2+r^4)} & \frac{2Mr^3(ry-ax)}{(a^2+r^2)(a^2z^2+r^4)} & \frac{2Mr^3(ay+rx)}{(a^2+r^2)(a^2z^2+r^4)} & \frac{2Mr^3(ay+rx)(ry-ax)}{(a^2+r^2)^2(a^2z^2+r^4)} \\ \frac{2Mr^3(ry-ax)}{(a^2+r^2)(a^2z^2+r^4)} & \frac{2Mr^3(ay+rx)(ry-ax)}{(a^2+r^2)^2(a^2z^2+r^4)} & \frac{2Mr^3(ry-ax)^2}{(a^2+r^2)^2(a^2z^2+r^4)} + 1 & \frac{2Mr^2z(ry-ax)}{(a^2+r^2)(a^2z^2+r^4)} \\ \frac{2Mr^2z}{a^2z^2+r^4} & \frac{2Mr^2z(ay+rx)}{(a^2+r^2)(a^2z^2+r^4)} & \frac{2Mr^2z(ry-ax)}{(a^2+r^2)(a^2z^2+r^4)} & \frac{2Mr^2z(ry-ax)}{(a^2+r^2)(a^2z^2+r^4)} + 1 \end{pmatrix}$$

This shows the many off-diagonal elements and complexity of the metric. Especially the expression for r leads to long partial derivatives when calculating the Christoffel symbols. The Mathematica code of paragraph 3.3 does however still produce the correct geodesic equations. Because this system of differential equations is multiple pages long it is not given here. There exist ways to optimize this systems and lower the number of floating point calculations needed [2]. This leads to less computation needed but the same results, so for the limited time of this thesis was not deemed necessary.

Ray tracing in curved space

4.1. Ray tracing

Ray tracing is a technique in 3D graphics to create a 2D projection of a 3D scene. It is generally a more computationally intensive method of rendering than more common methods but allows for more realistic lighting effects. We will be using ray tracing because this technique can also be extended to images in curved spaces where light does not travel in a straight line.

The ray-tracing process starts by placing a camera in your virtual scene, in front of this camera a virtual screen is projected. Now we can trace a ray starting from the camera going through the pixel of the virtual screen and continuing into the scene. Using vector calculus we are able for every object in the scene to calculate if there is an intersection between the object and the light path. This intersection point then determines the colour of the pixel given on the virtual screen. This process is illustrated in figure 4.1.

The implementation of this ray-tracing algorithm was made by following the excellent ebooks *Ray Tracing in One Weekend* [7] and *Ray Tracing: The Next Week* [8] of Peter Shirley. These books give a very detailed and step-by-step approach to implementing the code allowing for a solid structure and a great understanding of the code. This formed a solid basis which was later extended for curved spaces. The code is written in C++ which is compiled straight to machine code giving better performance than higher-level programming languages like Python and Matlab. These higher-level languages often do have libraries which are written using faster protocols but this limits the flexibility of the implementation.

The ray tracer has two different objects which can be placed in the scene, spheres and flat squares. Checking for intersection with a sphere can be done by finding the root of a quadratic equation. Checking for an intersection with a square can be done by finding the intersection point with the plane con-

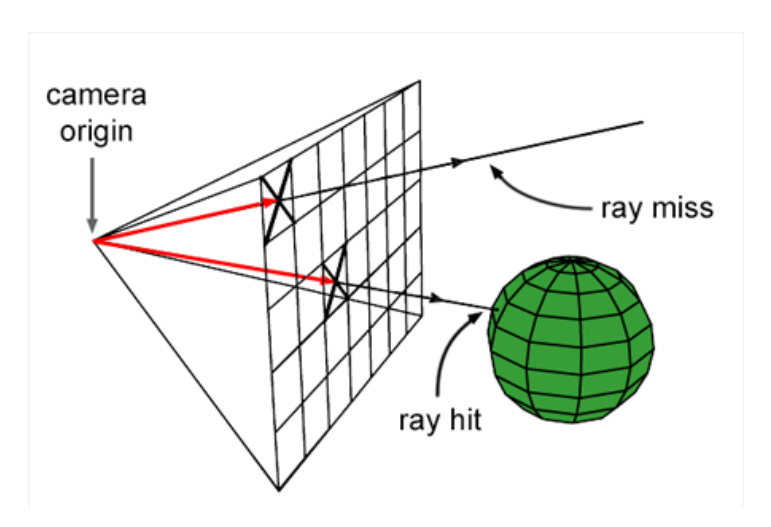


Figure 4.1: Graphic from the scratchpixel.com blog illustrating the ray tracing process

4.1. Ray tracing

taining the square and then checking if this point lies on the square. Another feature of the ray tracer is that two different materials are implemented. The first material has Lambertian reflectance, which means that a light ray reflects diffusely using Lambert's cosine law. When a light ray hits the object it is reflected off the object in the direction which is chosen randomly in a circle tangent to the point of impact. This kind of reflectance leads to an object that has a matt appearance. By recursively following the light ray bouncing off the object and letting every bounce influence the colour of the pixel, shadows appear in the image because light can then be blocked by objects. The other material implemented is a light-emitting material. This material only gives off light, so light bounces are not registered and when a light ray hits it the path is ended there. This process is illustrated in the following piece of pseudocode. Where ray is a vector with a position and a direction.

```
Algorithm 1 Basic ray tracing algorithm
```

```
for i \leftarrow 0, imageHeight do
   for j \leftarrow 0, imageWidth do
       ray \leftarrow GetRay(i, j, cameraPosition)

    Generate ray trough screen

       Image[i][j] \leftarrow PixelColor(ray)

    Color pixels of image

   end for
end for
function PixelColor(ray)

    Recursive function for bouncing ray

   for all object ∈ objects do
       if Hit(ray, object) then
                                                                                     • When ray hits, scatter
           scatterdRay ← Scatter(ray, object)
           return object.color(ray) * PixelColor(scatterdRay)
       end if
   end for
   return BackgroundColor(ray)
                                                                              • No further hits, exit recursion
end function
```

To avoid hard edges in the picture and average out the hard random noise of the Lambertian scatters it is possible to sample the pixels multiple times with a small random offset. At this stage, the program can generate the following scene of figure 4.2 filled with coloured Lambertian balls against a blue sky background.

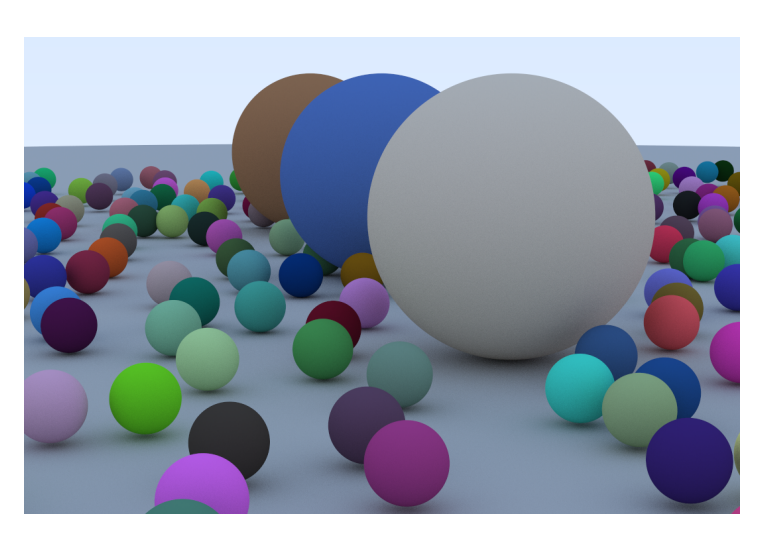
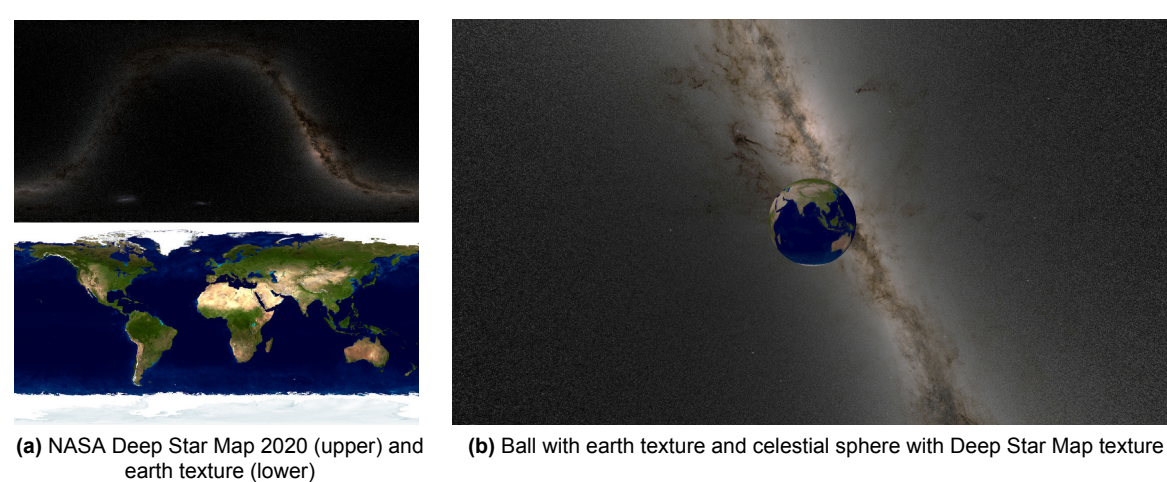


Figure 4.2: Image of Lambertian spheres generated by the ray tracer in flat space

To generate more realistic images, the textures of objects are necessary. The previously explained code used solid colours for the objects, but to add textures to the object we can map the point of intersection with the light ray to a location on a texture image. By centring a ball around the camera position with the texture of NASA's Deep Star Map 2022 [11] we can project the milky way realistically. A ball with Earth's texture was added to make the composition of figure 4.3.



cartif texture (lower)

4.2. Extending ray tracing to curved space

Figure 4.3: Combining Textures to create a image of earth in front of the milky way

The big difference between ray tracing in curved space is that the light rays do not travel in a straight line. Since light rays travel at the constant speed of light and do not undergo any acceleration they travel along the geodesics of chapter 3 that have the Minkowski metric $\eta = 0$ locally everywhere. To find the paths in the Schwarzschild case of a single mass point we can use either the series of differential equations from paragraph 3.3 or of paragraph 3.4. Because of the previously stated benefits, we will use the latter. For the Kerr case of a rotating black hole, we will use the differential equations derived from paragraph 3.5. We now need to set up the initial conditions for the light rays. If we are far enough away from the mass object the curvature will decrease and the space will be approximately Minkowski. This means that we can approximate the position and orientation of the light rays by the ones produced in the previous algorithm in Euclidean space. They all start at the camera so for the x, y, z coordinates we must choose the coordinates of the camera position. The time variable t can be chosen arbitrarily so we will use t = 0. For the velocities we will insure the speed of light in the initial conditions, this is done by choosing the velocities such that $\eta = 0$. For each pixel i, j we calculate the velocities such that they point on the virtual screen of the original ray tracing algorithm from section 4.1. This velocity is then normalized such that $\dot{x}^2 + \dot{y}^2 + \dot{z}^2 = 1$. In the ray-tracing process we follow the light ray in a backward direction, to do this and insure the speed of light we will use $\dot{t}=-1$. So the initial conditions can be written for every pixel i, j as

$$\begin{aligned} x_{i,j} &= x_{\mathsf{camera}} & \dot{x}_{i,j} &= \frac{x_{pixel(i,j)}}{||(x_{pixel(i,j)}, y_{pixel(i,j)}, z_{pixel(i,j)})||^E} \\ y_{i,j} &= y_{\mathsf{camera}} & \dot{y}_{i,j} &= \frac{y_{pixel(i,j)}}{||(x_{pixel(i,j)}, y_{pixel(i,j)}, z_{pixel(i,j)})||^E} \\ z_{i,j} &= z_{\mathsf{camera}} & \dot{z}_{i,j} &= \frac{z_{pixel(i,j)}}{||(x_{pixel(i,j)}, y_{pixel(i,j)}, z_{pixel(i,j)})||^E} \\ t_{i,j} &= 0 & \dot{t}_{i,j} &= -1 \end{aligned}$$

Now that we have the system of differential equations and initial conditions we can numerically integrate to get the path the light rays would travel. To do this the classic Runge–Kutta method was used because it has a reasonable accumulated error of $O(h^4)$ and is also used in other relativistic ray tracers [1].

We are now able to approximately get the points along the path of the light ray. It is not however possible to do ray tracing in an efficient way along a curve. So the light path is approximated by line segments in between the points on the curve as illustrated in figure 4.4, where the black line is the path of light and the red lines are used by the ray tracer. The program finds the intersection of the ray with any of the objects, if this intersection lies between the two points the colour of the object on that point will be adapted. In figure 4.4 this is illustrated by the upper curve hitting the ring around the black hole. To stop the ray from travelling indefinitely two stopping conditions are implemented. The first one is if the ray intersects with a black sphere at the Schwarzschild radius. Light is not able to escape this sphere and the original pixel becomes black. This is illustrated in the lowest light ray of figure 4.4. The second stopping condition is if the ray hits the background sphere around the black hole. If this is the case the angle of the light ray when it hits the sphere determines the position on the textured sphere that is sampled. This simulates the background sphere having an infinite radius, illustrated by the middle light ray of figure 4.4.

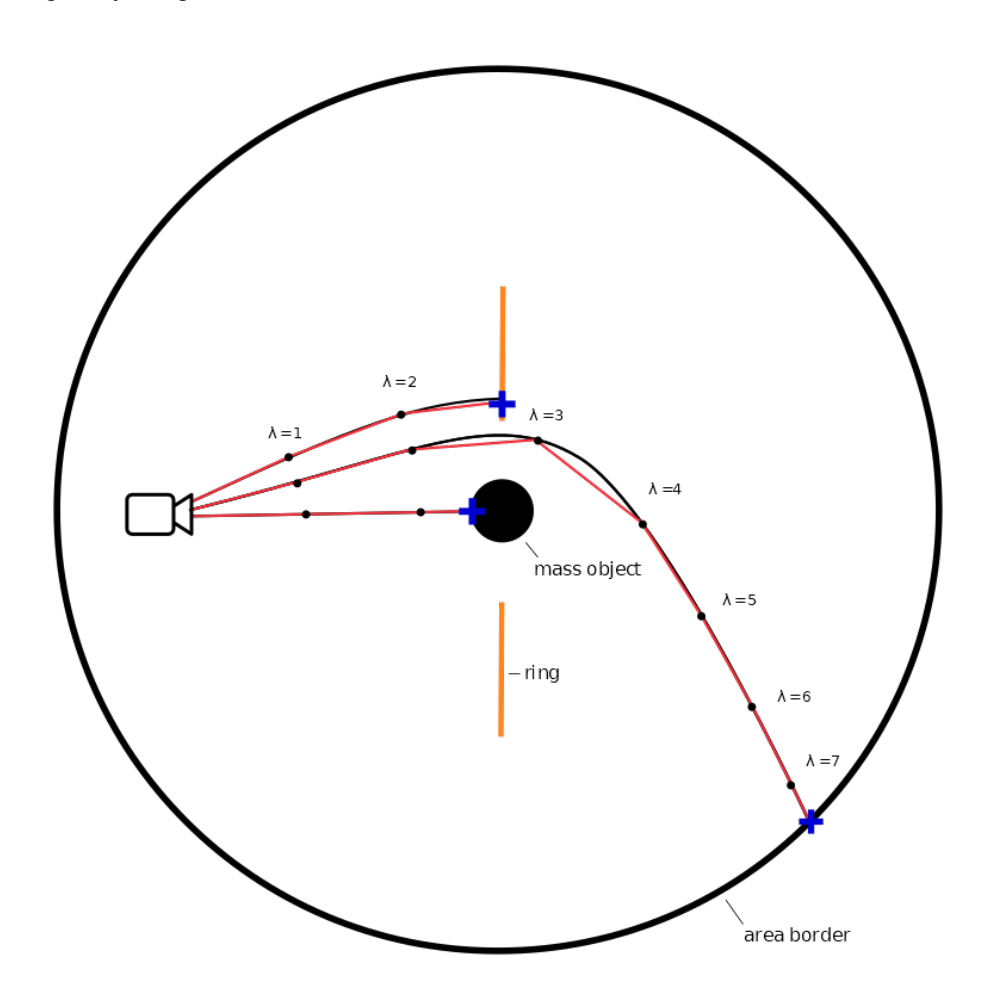


Figure 4.4: The ray-tracing process illustrated in 2D. Where 3 different geodesics are black and there linear approximations in red at every integer value of the progress variable λ . The upper geodesic hits the ring around the black hole, the middle one hits the celestial sphere and the lower one hits the Schwarzschild radius sphere.

end function

The program follows the following pseudocode to generate the images. For every pixel, the Pixel-Color algorithm is called which recursively steps over the curve and checks if it has not intersected any of the objects or satisfied any of the stopping criteria in between.

```
Algorithm 2 Ray tracing algorithm in curved space
n \leftarrow 100

    Set maximum number of steps

for i \leftarrow 0, imageHeight do
   for j \leftarrow 0, imageWidth do
       X \leftarrow SetX(i, j, cameraPosition)
                                                                                         · Set initial conditions
       Image[i][j] \leftarrow PixelColor(X, ray, n)

    Color pixels of image

   end for
end for
function PixelColor(X, ray, n)
                                                                        • Recursive function for bouncing ray
   X \leftarrow \mathsf{RK4\_Step}(X)
   ray \leftarrow UpdateRay(ray, X)
   for all object ∈ objects do
       if Hit(ray, object) then
                                                                                       • When ray hits, scatter
           X, scatterdRay \leftarrow Scatter(ray, object, X)
           return object.color(ray) * PixelColor(X, scatterdRay, n)
       end if
   end for
   if d(blackHole, ray) > 12 * r_{Schwarzschild} then
       return BackgroundColor(ray)
                                                                               · Limit reached, exit recursion
   end if
   if n < 0 then
       return errorMessage
                                                                                • Too little steps, exit program
   end if
   return PixelColor(X, ray, n-1)
                                                                                      • Not stopped, next step
```

4.3. Resulting Images

Now that we have adjusted the ray tracer to make use of the curved light paths we can generate images of virtual black holes. Figure 4.5 shows the results of an image generated by the algorithm. It is the Schwarzschild case using Kerr-Schild coordinates with the properties G = M = 1 resulting in a black hole with a Schwarzschild radius of 2. The background is NASA's Deep Star Map [11]. The curvature is clearly visible in the picture, the milky way in the background can be seen to the left of the black hole as well as to the right. This is because light rays originating from the milky way can both curve around the black hole from the left side of the black hole or the right side and hit the camera. So the same "picture" can be seen from different angular locations. Around the black hole, multiple rings are visible which correspond to light rays making consecutive orbits and ending up at the camera position where a small change of the exit angle can make the difference between 3 or 4 orbits around the black hole.

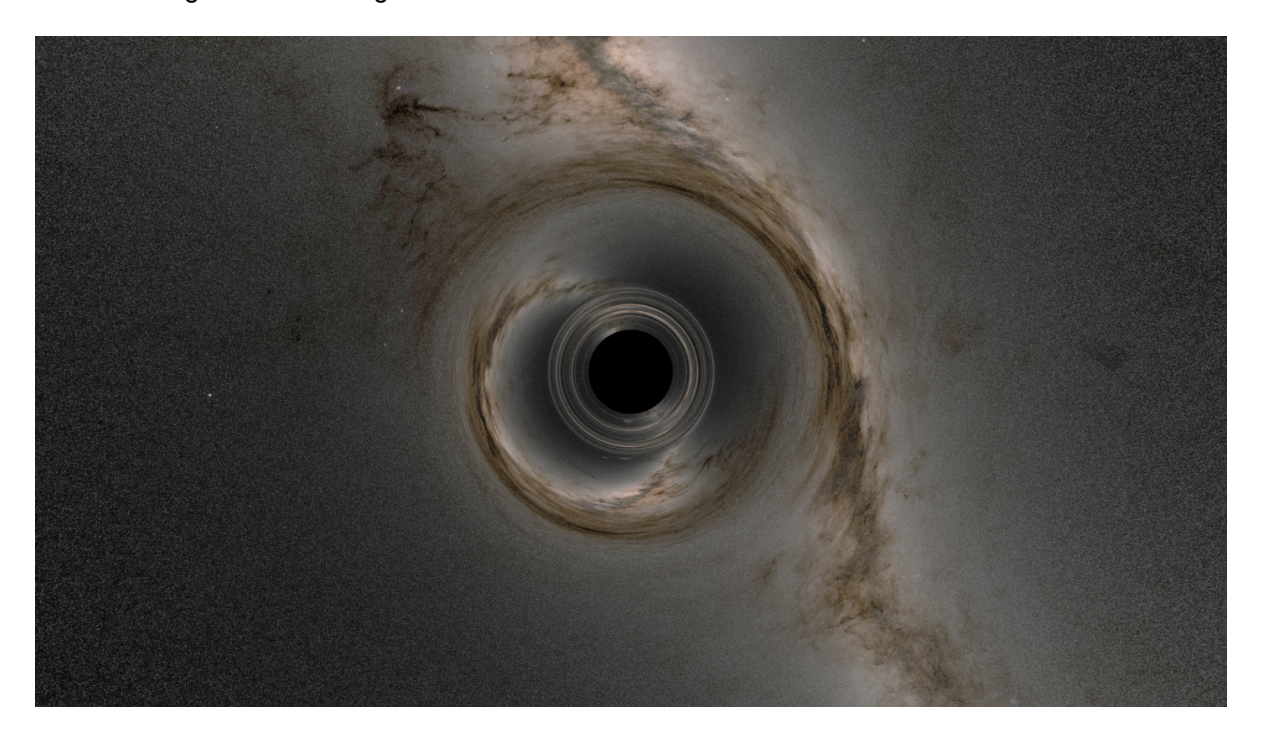


Figure 4.5: Schwarzschild black hole in front of the milky way with M=1, G=1 and NASA's Deep Star Map as the celestial sphere. The curvature leads to multiple projections of the milky way background around the black hole. The image is 1080 pixels high and has 8 samples per pixel.

Just like stars and planets, black holes can have particles orbiting them. These particles form the accretion disk surrounding the black hole. This accretion disk is filled with fast-moving and high-energy particles thus emitting light. To model the accretion disk a 2D circular texture was added around the black hole that emits light. The light emitted by the accretion disk overshadows the background light, so the celestial sphere will be solid black. The innermost stable orbit is the smallest orbit for which matter can have a stable circular orbit around the black hole. This determines the inner circle of the accretion disk, and for a non-rotational black hole is equal to $3 \cdot r_{\text{Schwarzschild}}$. There is no limit on the size of the accretion disk outer radius, but a radius of $8 \cdot r_{\text{Schwarzschild}}$ was chosen. The texture used for the simulation can be seen in figure 4.7. The result of the simulation can be seen in figure 4.6. The back side of the accretion disk is visible as the light rays originating from the disk can travel in a curved path over the black hole and reach the camera. Multiple smaller versions of the disk are visible around the black hole as light travels in multiple circles around the black hole and ends up at the camera.

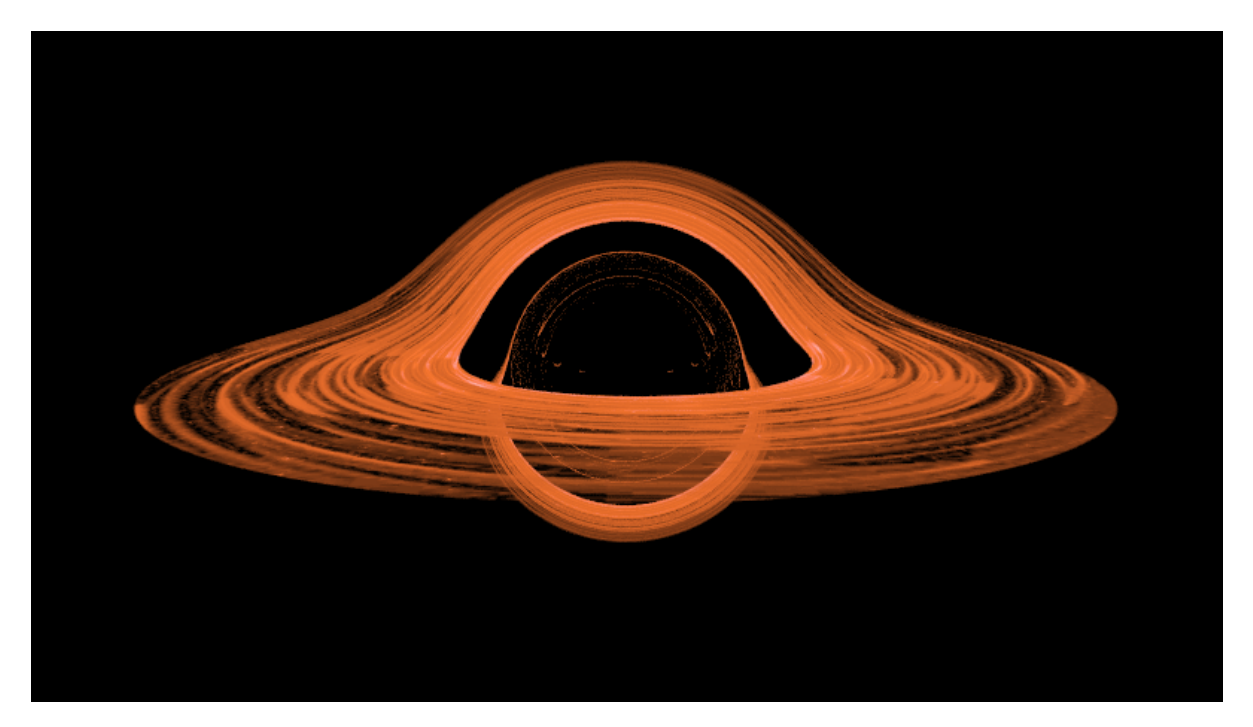


Figure 4.6: Schwarzschild black hole with M=1, G=1, a black celestial sphere and the accretion disk from figure 4.7. The accretion disk has a inner radius of $3 \cdot r_{\text{Schwarzschild}}$ and an outer radius of $8 \cdot r_{\text{Schwarzschild}}$. The image is 800 pixels high and has 16 samples per pixel.



Figure 4.7: Texture for the accretion disk consists of an orange ring with varying opacity simulating different brightness levels.

We can now also use the geodesic paths from paragraph 3.5to simulate a Kerr black hole. The camera position, location of the accretion disk, M, and G will remain the same but we will have rotation parameter a=0.99 instead of 0. This rotation will cause extra curvature of space-time, visible in the asymmetry of the image. Where the left side of the accretion disk appears longer than the right side and the shadow of the black hole has moved to the right. The image is only 400 pixels high and has 4 samples per pixel instead of 800 and 16 respectively. This is because the render time was much longer using the full Kerr metric. Even with the lower image quality settings figure 4.8 took over 2 hours to render whereas the render process for figure 4.6 took only a few minutes.

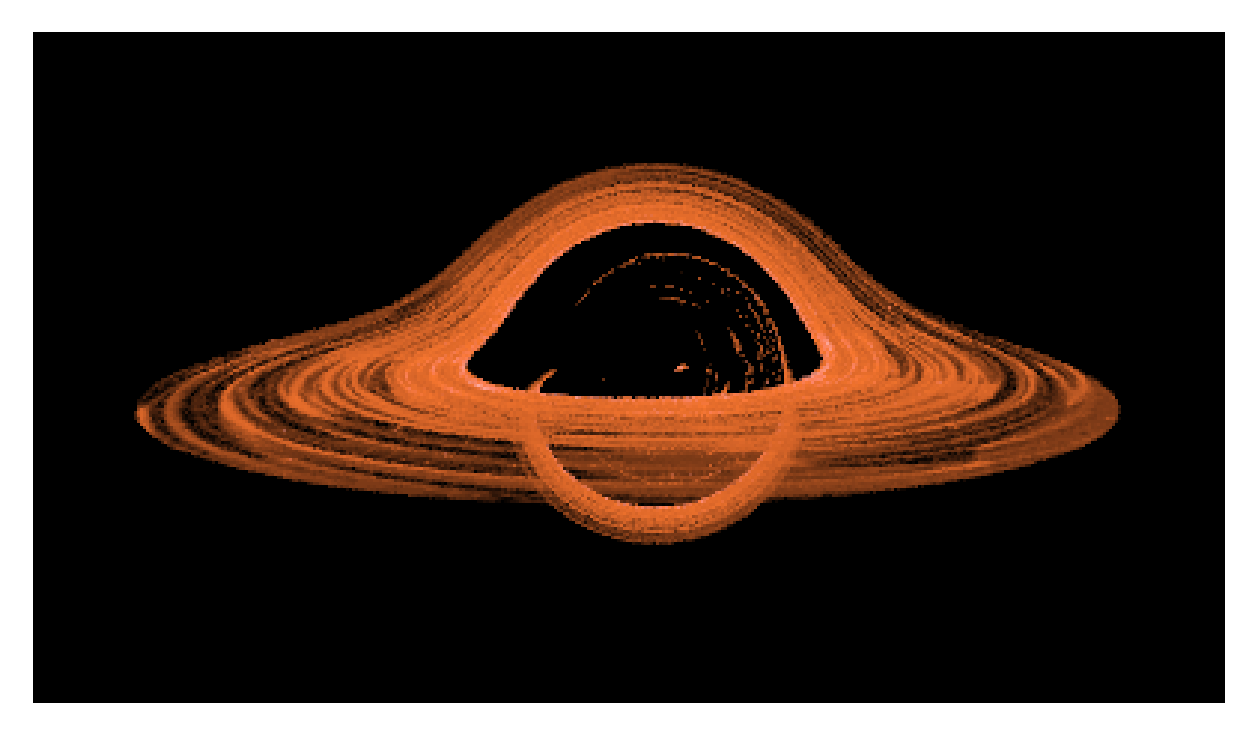
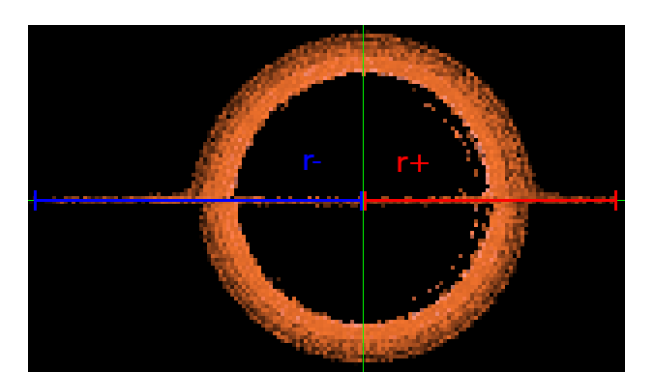


Figure 4.8: Kerr black hole with M=1, G=1, a=0.99, a black celestial sphere and the accretion disk from figure 4.7. The accretion disk has a inner radius of $3 \cdot r_{\text{Schwarzschild}}$ and an outer radius of $8 \cdot r_{\text{Schwarzschild}}$. The image is 400 pixels high and has 4 samples per pixel.

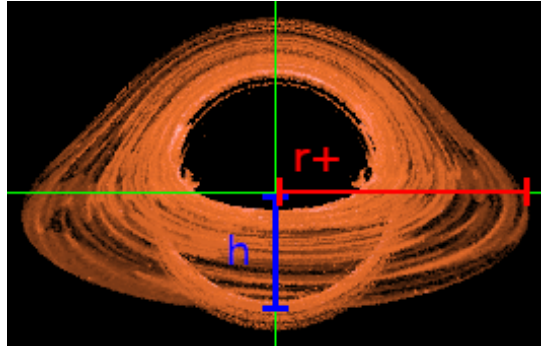
again

Fitting the parameters of a Kerr black hole

Because of the curvature of space-time and the distortion of light rays by this curvature, it is not trivial to estimate the parameters of an observed black hole. A way to still be able to get these parameters is to simulate the observed black hole and compare this simulated black hole with the actual black hole. We will assume that we have a picture of the observed black hole, the mass of the black hole and the radius of the accretion disk. The two parameters we want to estimate are the angular momentum of the black hole and the inclination of the accretion disk.



(a) Edge on view of a Kerr black hole with M=1, G=1, a=0.95, $\phi=\frac{\pi}{2}$ and an accretion disk with outer radius $3 \cdot r^{Schwarzschild}$.



(b) Schwarzschild black hole with M=1, G=1, $\phi=\frac{3\pi}{7}$ and an accretion disk with outer radius $3 \cdot r^{Schwarzschild}$.

Figure 5.1: r^+ : In red the distance from the centre of the black hole shadow to the right edge of the disk. r^- : In blue the distance from the centre of the black hole shadow to the left edge of the disk. h: In blue the distance from the centre of the shadow to the lower edge of the disk.

We assume that the plane of rotation of the black hole is the same as that of the accretion disk. To measure the angular momentum we must have a side view because there are no asymmetries in the plane tangent to the accretion disk. We define r^+ and r^- as in figure 5.1 (a). The ratio between r^+ and r^- are now be used to estimate the rotation parameter a. In the following table the values for r^+ and r^- are given in pixels for the case M=1, G=1, we are looking at the black hole in the plane tangent to the accretion disk and the disk had a diameter of $6 \cdot r_{\text{Schwarzschild}}$. Which is small for an accretion disk but allows us to measure using a low-resolution simulation.

The curvature caused by the rotation of the black hole results in unequal lengths r^- and r^+ . In this case we have a relation between the rotation $\frac{a}{M}$ ratio and the ratio between r^+ and the total diameter

 $[\]frac{r^+}{r^-+r^+}$ that seems linear.

$\frac{a}{M}$	r^- (pixels)	r^+ (pixels)	$\frac{r^+}{r^-+r^+}$
0,00	76	76	0,500
0,20	77	72	0,517
0,40	79	71	0,527
0,60	80	69	0,537
0,80	86	67	0,562
0,90	85	65	0,567
0,95	87	65	0,572

To measure the inclination of the accretion disk we can use the ratio between r^+ and h as defined in figure 5.1. In non-curved space, we would expect this ratio to be equal to $\cos(\phi)$ where ϕ is the angle of the inclination. In curved space, this is however not true and we can use the black hole visualisation to get the actual values. In this simulation the parameters where M=1, G=1, a=0 and the diameter of the accretion disk was again $6 \cdot r_{\text{Schwarzschild}}$.

of the accretion disk was again $6 \cdot r_{\text{Schwarzschild}}$. The ratio $\frac{h}{r^+}$ gives values for ϕ that are higher than the expected $\cos(\phi)$. The ratio is the same as $\cos(\phi)$ at $\phi=0$ and $\phi=\frac{\pi}{2}$ but is higher in between.

ϕ	h (pixels)	r^+ (pixels)	$\frac{h}{r^+}$	$\cos(\phi)$
$\frac{0\pi}{14}$	90	89	1,01	1,00
$\frac{14}{14}$	95	90	1,06	0,97
$\frac{14}{2\pi}$	98	90	1,09	0,90
$\frac{14}{3\pi}$	97	91	1,07	0,78
$\frac{\frac{14}{4\pi}}{14}$	87	91	0,96	0,62
$\frac{14}{5\pi}$	69	91	0,76	0,43
$\frac{14}{6\pi}$	38	93	0,41	0,22
$\frac{\frac{14}{7\pi}}{\frac{14}{14}}$	0	91	0,00	0,00

These ratios can be hard to pinpoint for combinations of non-zero inclination and rotational momentum but illustrate the ability to study astronomical observations of a black hole with the pictures generated by the ray tracing algorithm.



Conclusion

In this thesis, the mathematics and ray racing algorithm for generating images of a Kerr black hole with an accretion disk in a celestial sphere where studied and implemented. This allowed us to create amazing visualisations of black holes. There are however still limitations to the implemented approach.

One of the assumptions made is the shape and texture of the accretion disk that surrounds the black hole. This shape was assumed to be a flat circle with a hole in the middle. The actual structure of a black hole's accretion disk could be more complicated. The accretion disk of an actual black hole would also have asymmetries in colour and brightness because of the Doppler effect, this is however not modelled in this thesis.

The second main limitation is the speed of the algorithm. Especially rendering an image of a rotating Kerr black hole can take hours because of the number of calculations needed to numerically integrate the multi-page system of differential equations. There are shorter ways to write the system and these could be implemented. An additional way to decrease the render times is to implement parallel computing. Multiple calculations of pixel colour can be done in parallel on different computer cores to significantly increase the speed of the progress.

Acknowledging the shortcomings of the model, it can still be useful to study the properties of observed black holes. In the future, we expect to get higher-resolution images of black holes. We can then use these images to estimate the inclination of the accretion disk and the angular momentum of the black hole. The ray tracing model also makes it plausible to see if our mathematical models of a black hole are correct and discover the structure of the material surrounding the black hole in the accretion disk. Making ray tracing in curved space-time a essential tool to study the effects of general relativity such as objects like black holes



Code

The code for this thesis with instructions for building and running is available at: $\verb|https://github.com/thomaskamminga/RayTracingUsingRelativity|$

Bibliography

- [1] Chi-kwan Chan. Ray Tracing: Interfacing Black Hole Theory and Observations. 2020. url: http://bhpire.arizona.edu/wp-content/uploads/2020/10/2020-10-27_Ray-Tracing Reduced.pdf.
- [2] Chi-kwan Chan et al. "GRay: A General Purpose Geodesic Integrator for Kerr Spacetimes". In: *The Astrophysical Journal* 867.1 (Oct. 2018), p. 59. doi: 10.3847/1538-4357/aadfe5. url: https://doi.org/10.3847/1538-4357/aadfe5.
- [3] Jean-Pierre Francoise, Gregory L. Naber, and Tsou Sheung Tsun. *Encyclopedia of Mathematical Physics*. Academic Press, June 2006.
- [4] Bas Janssens. Course AM3580 Introduction to differential geometry. Academic Year 2021/2022. Delft University of Technology, 2021.
- [5] Steven R. Lay. "Section 6 Metric spaces". In: *Analysis: With an introduction to proof.* Pearson Education, 2014, pp. 158–159.
- [6] Renaud Raquépas and Erick Schulz. "Topics Geometry and Topology–MATH 599 Visualization of Kerr black holes". In: (2017).
- [7] Peter Shirley. Ray Tracing in One Weekend. Dec. 2020. url: https://raytracing.github.io/books/RayTracingInOneWeekend.html.
- [8] Peter Shirley. Ray Tracing: The Next Week. Dec. 2020. url: https://raytracing.github.io/books/RayTracingTheNextWeek.html.
- [9] Erik Tollerud. Kerr Orbit GR Project. [Online; accessed 2022-06-08]. June 2007. url: https://www.physics.uci.edu/etolleru/KerrOrbitProject.pdf.
- [10] Matt Visser. "The Kerr spacetime: A brief introduction". In: *The Kerr Spacetime: Rotating Black Holes in General Relativity*. Cambridge University Press, 2008.
- [11] Ernie Wright. SVS: Deep Star Maps 2020. en. publisher: NASA. Sept. 2020. url: https://svs.gsfc.nasa.gov/4851.